ASSESSMENT OF WIND TURBINE BLADE TRAILING EDGE FAILURE WITH SUB-COMPONENT TESTS

F. Lahuerta[1], M. J. de Ruiter[1], L. Espinosa[1], N. Koorn[1], D. Smissaert[1]

[1] Knowledge Centre WMC. Kluisgat 5, 1771 MV Wieringerwerf, The Netherlands

Keywords: wind blade, adhesive, sub-component, buckling, edge moment, trailing, failure

ABSTRACT

Wind turbine blades present different types of failure mechanisms which are associated with specific loading modes. Trailing edge failure is driven by delamination and buckling of the trailing edge adhesive joint of a wind turbine blade under edge moments. Such failure mode has been invoked in and well-documented for full-scale blade tests and for undesirable failures of blades on service. This paper describes a test set-up for a blade sub-component aimed at achieving trailing edge failure after buckling, which is an improvement in the experimental verification of a blade design. The description of the test setup and static test results are reported. Experimental results are discussed and compared with a FE model to describe the failure mechanism.

1 INTRODUCTION

One of the main cost drivers in wind energy sector is operation and maintenance costs (O&M). The normalised downtime caused by blade failures and blade O&M action has been evaluated between 3% to 10% by different studies [1]–[3]. Among the different types of blade failure modes described by Attaf [4], Ataya [5] reported the failure of the adhesive trailing edge as one of the main issues concerning the reliability of blade designs due to failures and downtimes.

Eder [6] described the fracture problem of trailing edge adhesive joints where the most critical failure mode seemed to be Mode I contribution due to the opening of the trailing edge. Moreover, a method to estimate the SERR (strain energy release rate) of all fracture modes in the trailing edges of large wind turbine rotor blade models was proposed [7]. Blade tests performed by DTU Risø [8] for a SSP 34 [m] blade suggested the trailing edge adhesive joint failure due to local buckling. In addition, an internal wire reinforcement for the SSP 34 [m] blade was implemented to prevent out-of-plane deflection of the panels, therefore reducing the peeling stress on the adhered region. Moreover, Branner & Haselbach [9] described the blade test trailing edge failure mechanism by an FE model which considered transverse shear stresses (by use of an 8-noded double curved thick shell element). It was found that buckling led to the trailing edge adhesive joint final failure well below the expected maximum load.

Carrying out full scale blade tests for the assessment of the buckling and fracture behaviour of the trailing edge is expensive and impractical. Full scale blade tests are performed at later stages of the design process for qualification purposes [10]. Sub-component tests are therefore more suitable for the study and design of local failure mechanisms as the trailing edge adhesive joint failure. Thick adhesive joint failures have been studied before using sub-component tests, i.e. in beam tests [11]. However, very few developments of sub-component test methods to study the trailing edge adhesive failures are available. Therefore, in the IRPWind project framework several institutions collaborated to develop sub-components test setups to asses trailing edge failure [12].

The aim of the work is to describe a test method which allows studying wind turbine blades trailing edge failures due to loading cases dominated by an edgewise moment. The test method allows testing full-scale segments of a blade or sub-components. Due to the edgewise bending moment loading case, trailing edge adhesive failure delamination is promoted. This case of failure mode is observed during

the tests and described by the FE models of the sub-component, where a buckling wave of the trailing edge is formed due to the compression introduced by the applied edgewise moment leading to a full delamination.

2 MATERIAL AND METHODS

The development of the test method was performed by WMC in the IRPWind project framework. Segments of a wind turbine blade were provided by DTU Risø and used as a development platform for the test method and further study of the trailing edge adhesive failure. In this work, the segment of the wind turbine blade at station Z=24m of 3 meters long, 2 meters wide and 400mm of maximum profile height were evaluated. Figure 1 shows the internal structure of the blade segment, where the thick laminate CAP and the shells sandwich panels which form the aerodynamical profile can be distinguished. Both shells panels are bonded with an adhesive thick joint at the leading and trailing edge.

Figure 1: Blade segment sub-component coupon

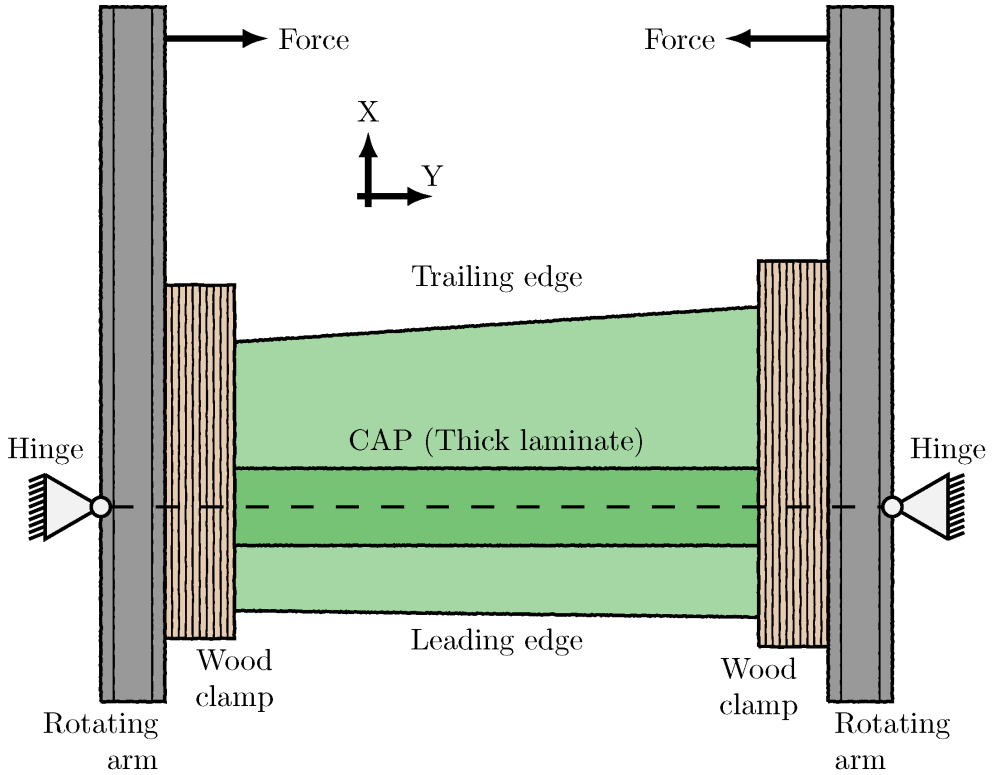

Figure 2: Scheme of the test method.

To apply an edge moment to the wind turbine blade segment in a sub-component test, initially a geometrical parametric model and boundary conditions was defined in FE. To define the edgewise moment it was necessary to state a rotation axis and an off-axis punctual load which creates the edge moment. The test setup was developed with a symmetry plane in the middle of the sub-component. The model scheme used for the test definition is described in Figure 2. The model scheme includes the following parts and parameters:

- The segment of the blade or *sub-component* coupon, which is obtained directly by sectioning a blade in parts of a certain sub-component length.
- The *wood clamp reinforcements*, which allow introducing the load exerted by the test frame to the sub-component. The load or moment applied by the loading arms is transformed into a shear load by the reinforcement clamps. This shear load is distributed along the surface of the sub-component clamping areas with the help of a low elastic modulus adhesive paste. These areas are defined by the clamp overlap length parameter.
- The *rotating arms*, which are defined by the position of the rotation axis (or *hinge*) and the length between the rotation axis and the point where the load is applied by the actuator.

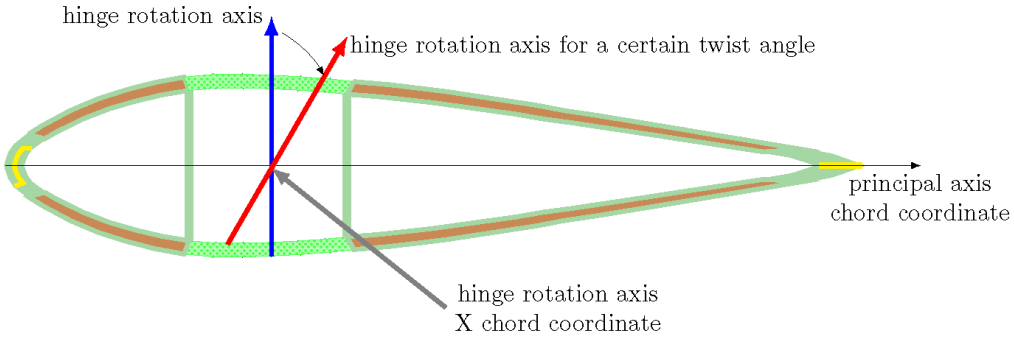

Figure 3: Sub-component scheme side view.

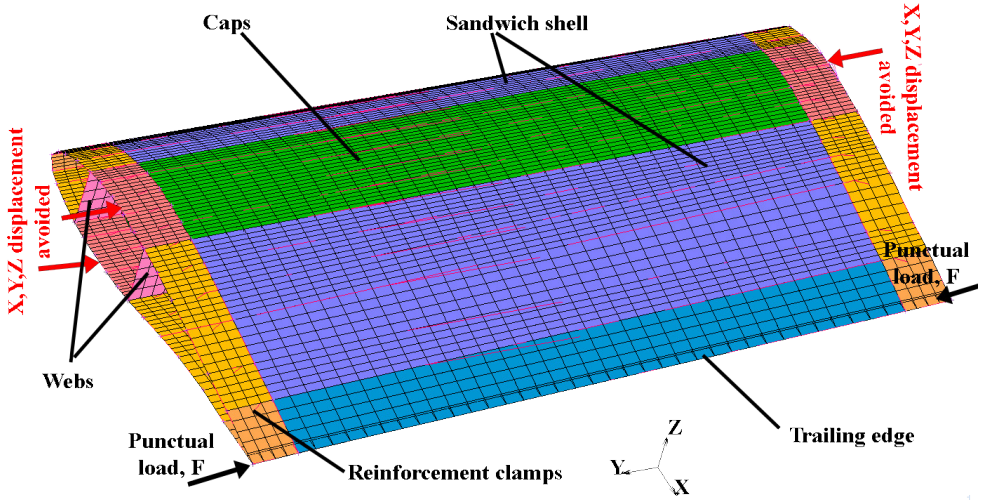

Figure 4: Sub-component FE model.

The rotating arms impose an edge moment on the sub-component. The position of the rotation axes determines where the neutral line of the corresponding bending displacements is located. Furthermore, the position determines the distance to the load actuator. This distance, multiplied by the actuator force, is the imposed edge moment. Figure 2 shows that the rotation axes are positioned symmetrically at each side of the model, at certain X coordinate. This X coordinate is to be determined based on the strain distribution observed in a blade test [10], [13], [14] and the desired edge moment distribution. The strain distribution can be determined by the position of the neutral line of the blade profile, which is dependent of the inertia of the section. However, in general it can be assumed that the position of the

neutral line is close to the cap width middle position (in general, close to the middle of the UD thick laminate).

To add a flap moment contribution to the edge moment, the sub-component can be mounted at different angles around the Y axis formed by the line between the two hinges (see Figure 3). This allows to setup the sub-component test for a combined edgewise and flapwise bending moment where strain distributions mimic multiaxial blade loads cases. However, in this work the test setup was performed with no flapwise contribution.

2.1 Sub-component FE model description

A FE model was build according to Figure 2 using 2D quad shell elements in MSC Marc. The FE model was divided in different regions with material properties and thicknesses according the sub-component structure shown in Figure 4. The thick laminate Cap regions were modeled as a variable thickness of 24mm to 38mm distributed along Y elements with a layout [Biax,UD,Biax]. The sandwich regions were modeled with thicknesses from 20 to 30mm with a [Biax, PVC, Biax] layout. Since the main purpose of the model was to compare the longitudinal strains and the buckling load with the experiments, dissipative modeling energy methods (i.e cohesive elements) were avoided. This assumption implies that it was not possible to model the failure load. Therefore, the regions located at the trailing edge and leading edge adhesive joints were modeled as a single line of nodes connecting the up-board and in-board shells with shell elements of a thickness of 5mm and a layout [Biax, Adhesive, Biax]. The regions of the reinforcement's clamps were modeled adding an extra thickness of 200mm of wood material to the layout to mimic the extra stiffness added by the clamps. Detailed dimensioning of the clamping size region was performed based on a detail study of the adhesive shear strength between the clamping wood blocks and the sub-component.

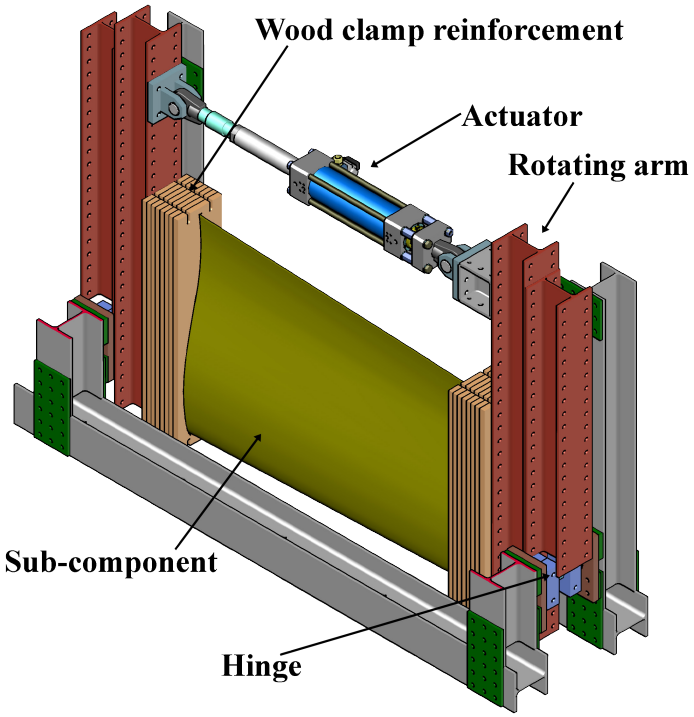

Figure 5: Sub-component test rig setup.

Material properties for Biax, UD, Adhesive and PVC were collected from properties reported for the original blade [15] from where the sub-components were obtained. Boundary conditions for the model were applied according to the scheme from Figure 2. To mimic a hinge at the CAP region middle node, fixed displacement boundary conditions were applied for the 3 translation degrees of

freedom and allowing the rotation for the three axes. Since on the position of the hinge stiffness was increased by the wood reinforcement, local artificial concentrations of stresses at the hinge position were not considered or transfered to the gauge section located between both reinforcements clamps. In order to determine the width of the reinforcement clamps, a sensitivity study for different widths was performed aiming to achieve stability for the buckling load [16]. In addition, a point load was added to the ultimate node of the trailing edge in both sides of the sub-component to create the edgewise moment. The local stress concentrations caused by the local point load were neglected, since the node belongs to the clamp region with a high stiffness. A linear incremental force was used for the point load.

2.2 Test setup description

A test rig was developed by WMC according the load conditions shown in Figure 2. The test rig was mounted with structural beam elements and clamped to the strong concrete floor available at WMC. The test rig comprises (see Figure 5) two symmetrical loading arms which can rotate due to a hinge attached between the rotating arms and the test rig frame structure. Both rotating arms are connected on the top by a 250kN hydraulic cylinder actuator which is controlled to perform static or fatigue tests. The rotating arms allowed bolting the reinforcement wood clamp bonded to the sub-component. In this way the sub-component can be positioned at any relative position, allowing varying the X-axis position of the hinge with respect of the sub-component chord or the hinge rotation axis angle described in Figure 3.

Sub-component coupons were provided by DTU and obtained from cutting a 34 meter wind turbine blade [8] in segments of 3 meters with no further preparation. Based on the measurements of the blade profiles at the extremes of the sub-component, cross laminated timber plates were cut with the aerodynamical profiles. The timber plates were stack together and bonded to the extremes of the subcomponent with a bonding paste forming the wood clamp reinforcements. Based on a FE sensitivity analysis a width of 320mm was chosen for the clamping width.

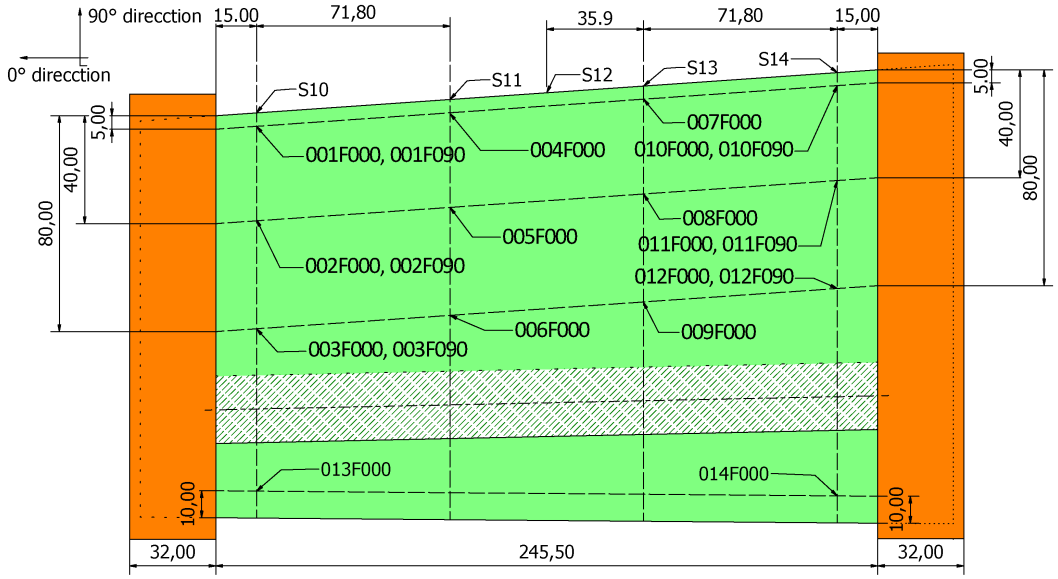

Figure 6: Sub-component instrumentation and dimensions diagram. Units in [cm].

The sub-component was instrumented with strain gauges of 5mm gauge section to measure the longitudinal strains and the transversal strains in several points. Figure 6 shows the position of the strain gauges on the surface of the sub-components, in-board and out-board surfaces were instrumented with the same layup of strain gauges. Strain gauges were positioned according a grid of 4 columns and 4 rows and labelled from position 001F000 to 014F000 were the last numbers refers to

the orientation (longitudinal or transverse strain). The grid instrumentation layout allowed plotting the longitudinal strains versus the X-axis position to visualize the evolution of the edge moment. In addition linear displacement sensors (S10 to S14) were placed perpendicular to the coupon leading edge to record the amplitude of the buckling wave formed due to the edgewise moment.

The coupon was loaded in a static test by contracting the actuator at a constant speed of 5mm/min until sub-component failure. The static test was recorded with cameras from different angles in order to visualize the trailing edge buckling wave and ultimate failure [17]. In addition a laser was positioned as referencing system to indicate the original position of the trailing edge. A displacement sensor and a load cell were mounted on the actuator. The edgewise moment was computed as the resultant of the force measured by the load cell and the distance between the hinge and the actuator position of 192 [cm]. The edgewise loading angle was computed by trigonometry based on the measurement of the actuator displacement sensor.

4 RESULTS AND DISCUSSION

4.1 Sub-component static tests results

The sub-component coupon was loaded with an edgewise moment at constant speed until failure. The test was characterised by the formation of a buckling wave along the trailing edge which promoted the full delamination of the trailing edge adhesive joint. During the static test three main stages were observed (see Figure 7, left): the pre-buckling, the post-buckling and the ultimate failure and delamination stage.

The *pre-buckling stage*. In this first stage the mechanical behaviour of the blade section was characterised by a linear edgewise stiffness until the buckling moment was achieved. The buckling wave during the pre-buckling stage was characterised by low amplitudes of the off XY plane displacements (see Figure 7 right).

The *trailing edge post-buckling stage*. In this stage it was observed a drop of the sub-component edgewise stiffness and a non-linear stiffness behaviour until the final failure. The loading position between the pre-buckling stage and the post-buckling stage showed an inflection point due to the change of the stiffness's. This inflection point was determined as the buckling point located at 1 degree of edgewise loading angle and an edgewise moment of 95 [kNm]. Beyond the buckling point and during the trailing edge post-buckling stage, the amplitudes of the buckling wave formed along the trailing edge showed a rapid increase leading to maximum amplitudes of 30 [mm] before the final failure (see Figure 7 right).

The *ultimate failure stage.* The failure was characterised by a sudden delamination failure of the trailing edge adhesive joint. The full delamination occurred at an edgewise moment of 142 [kNm], where a dramatic decrease of the edgewise stiffness was recorded once the trailing edge was delaminated. The failure occurred at the highest buckling wave amplitudes recorded.

Figure 8 shows the top view of the trailing edge during the test, where it is described how the buckling wave is formed at different levels of edgewise moments. While at 20% of the total edgewise capacity the buckling wave is barely visible, higher edgewise moments show higher buckling wave amplitudes until final adhesive delamination. The failure mechanism of the trailing edge adhesive joint is driven by the buckling wave formation. The increment of the buckling wave amplitude is associated with a multiaxial load state in the trailing edge adhesive joint, where the inboard and outboard panel tends to separate (also denominated as "the breathing of the blade") leading to higher peeling loads along the adhesive joint. Similar failure mechanisms have been reported for blade test [13], [14] and trailing edge blades failures on service [5], where due to the action of combined flapwise and edgewise moments adhesive joint failures were promoted. According to the failure mechanism recorded with the cameras [17] and strains distributions, the tests setup was able to mimic the loading conditions of an edgewise moment which drive the adhesive failure of the trailing edge.

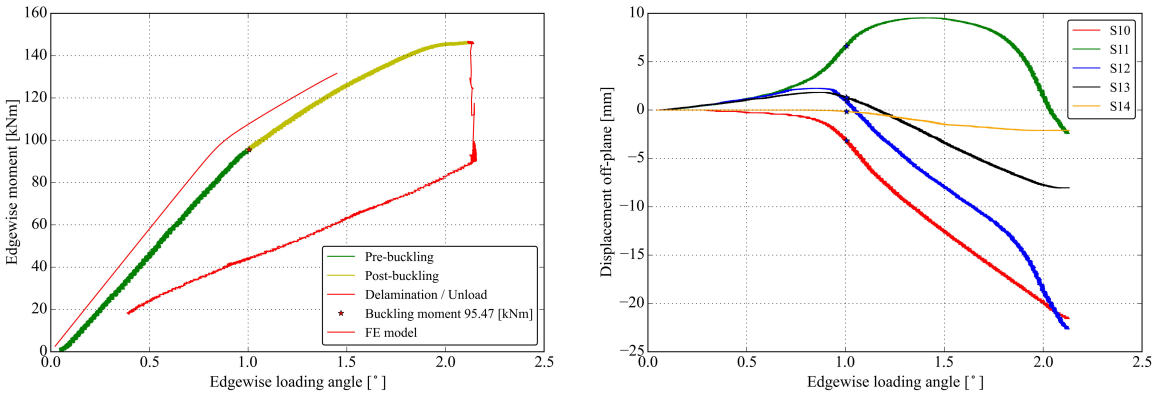

Figure 7: Edgewise moment versus edgewise loading angle of the rotating arms (left plot). Off XY plane displacements versus edgewise loading angle of the rotating arms (right plot), displacement sensors S10 to S14.

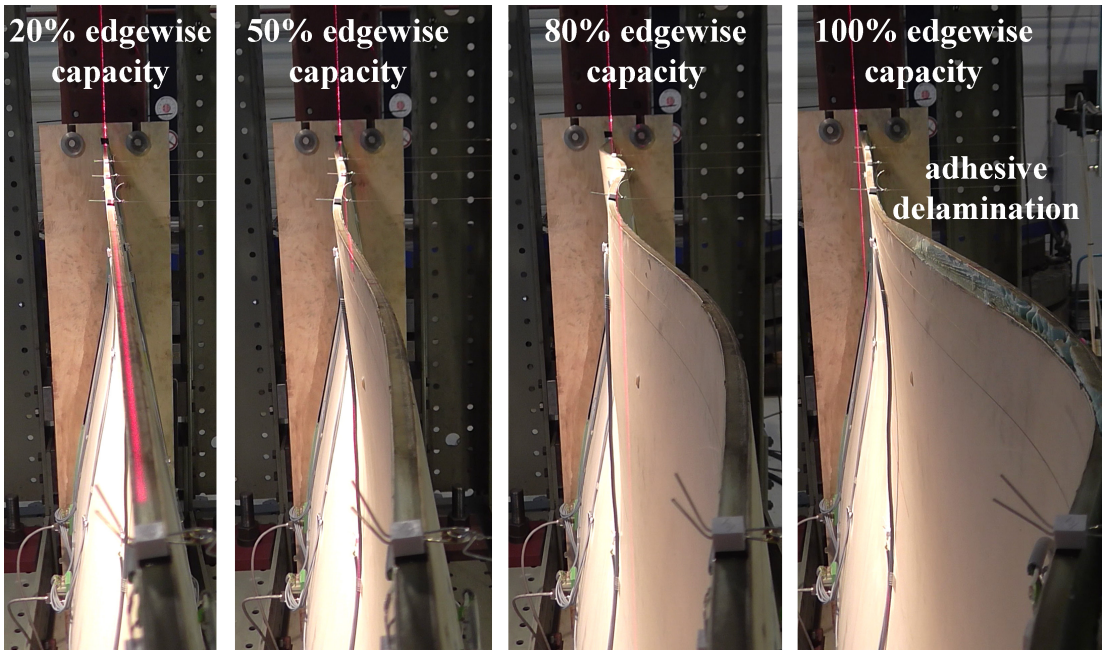

Figure 8: Side view of the trailing edge during the test. Buckling wave formation and adhesive joint delamination failure mechanism.

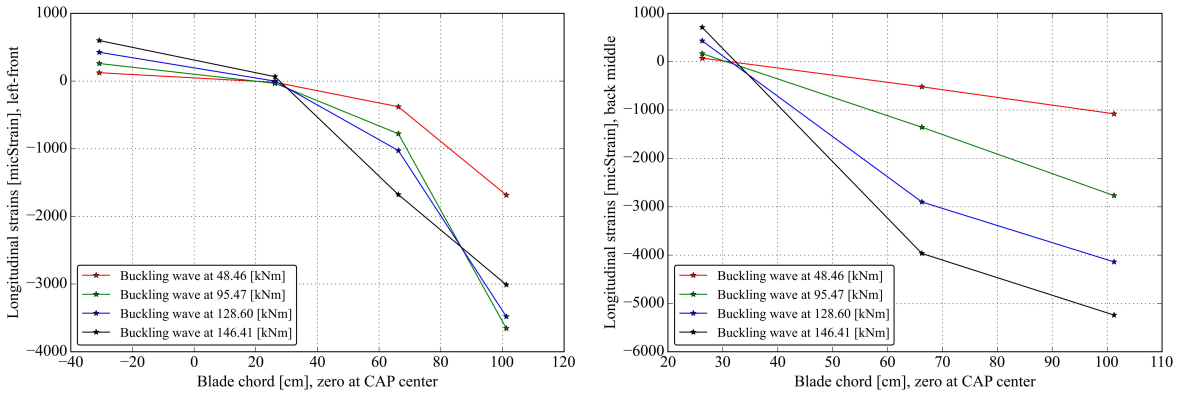

Figure 9: Longitudinal strain (in Y axis) versus chord position (X axis), strain gauges 001F000, 002F000, 003F000, 013F000 (left plot). Longitudinal strain (in Y axis) versus chord position (X axis), strain gauges 004B000, 005B000, 006B000 (right plot). Leading at -40 [cm] and trailing edge at 120 [cm].

Figure 9 describe the evolution of the longitudinal strains at different edgewise moments and across the blade chord. The longitudinal strains plotted across the blade chord are equivalent to the strain distribution that can be expected for an edgewise moment. Right and left figures show that longitudinal strains are distributed from maximum compression state at the trailing edge, to a minimum tension state at the leading edge. In addition, the longitudinal strain distribution shows null values for chord positions crossing the CAP location or neutral axis. The distribution of the longitudinal strains across the chord shows that the setup was able to mimic an edgewise moment stress distribution across the subcomponent. Maximum compression longitudinal strains of 6000 [micStrain] were recorded close to the failure and compression longitudinal strains of 3000 [micStrain] were recorded at the buckling load. Moreover, Figure 10 describes the evolution of the transverse and shear strain across the blade chord. Shear strains caused by the edgewise moment loading showed values of 6000 [micStrains] at the trailing edge position.

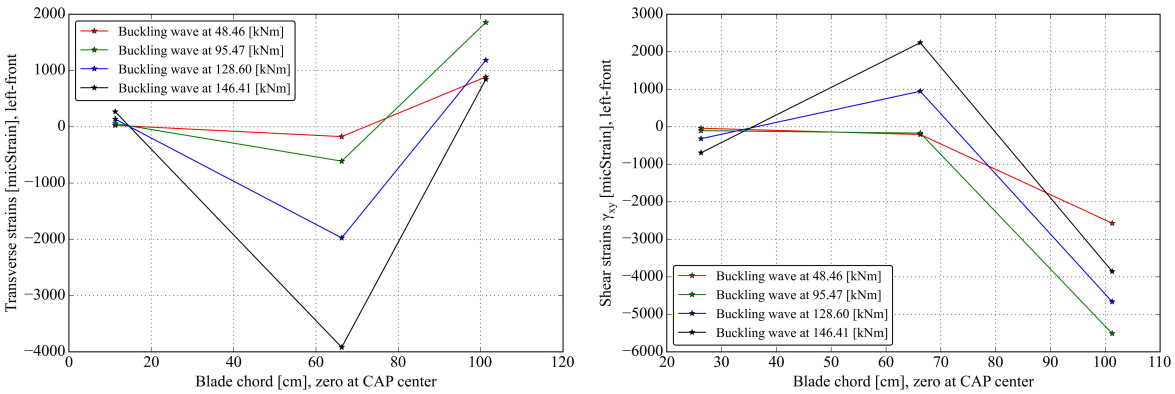

Figure 10: Transverse strain (in X axis) versus chord position (X axis), strain gauges 001F090, 002F090, 003F090 (left plot). Shear strain (in XY axis) versus chord position (X axis), rossete strain gauges 001F, 002F 003F (right plot). Leading at -40 [cm] and trailing edge at 120 [cm].

4.2 Sub-component FE modeling

The test setup was 2.5D modelled following the scheme described in Figure 2 and according to the specifications of section 2.1. Figure 11 shows the model deformed shape and maximum stress failure index. The model deformed shape shows a buckling wave on the third order located on the trailing edge, which is comparable with the one recorded during the static test (see Figure 8). Larger failure indexes values are located on maximum and minimum buckling wave peaks where multiaxial strain fields can be expected. The model suggests that the opening at the trailing edge (or breathing of the blade) cause by an edgewise moment can be related to the compression loads formed along the trailing edge. Figure 12 (right) shows the opening angle of the trailing edge plotted versus the edgewise loading angle, where the opening angle of the trailing edge was computed by trigonometry according to the displacements of inboard and outboard nodes. The figures describe the opening angle of the trailing age is intrinsically related with the pre-buckling and post-buckling stages. While during the pre-buckling stage the opening angle of the trailing edge shows weak dependence with the edgewise moment, once the post-buckling stage is achieved edgewise moment and trailing edge opening angle show a linear dependence. Moreover, large trailing edge opening angles can be related with the final delamination, due to the mode I fracture failure of the trailing edge adhesive joint. On this regards several publications have described similar reasons for thick adhesive joints failure from the point of view of fracture mechanics with experimental tests [6], [10], [18], [19] or with dissipative fracture mechanics FE models [7], [12], [14].

Based on the reaction forces and nodal displacements, the edgewise moments and edgewise loading angles were computed and plotted within the experimental data in Figure 7 (left) where FE model and experimental edgewise stiffness are shown. Figure 7 (left) shows a good agreement between

experimental and FE model, and in both is possible to observe the characteristic change of stiffness which defines the buckling point. The model represents the edgewise behavior of the sub-component or blade segment, a similar model can be obtained segmenting full blade models such as the ones generated by software packages such as FOCUS and applying similar boundary conditions. Since the blade profile is asymmetric and the loading vector does not coincide with the inertia axis of the section, the structure is unstable. Therefore, no further artificial boundary conditions were needed to promote the buckling behavior. Moreover, longitudinal strains recorded during the test and obtained with the FE model are showed in Figure 12 (left), where some differences can be observed in the local region of the trailing edge. However, both are comparable in term of value and shape, indicating that an edge moment is formed across the blade sub-component where the trailing edge is loaded in compression and the leading edge is loaded in tension limiting the position of the neutral line to the middle location of the CAP.

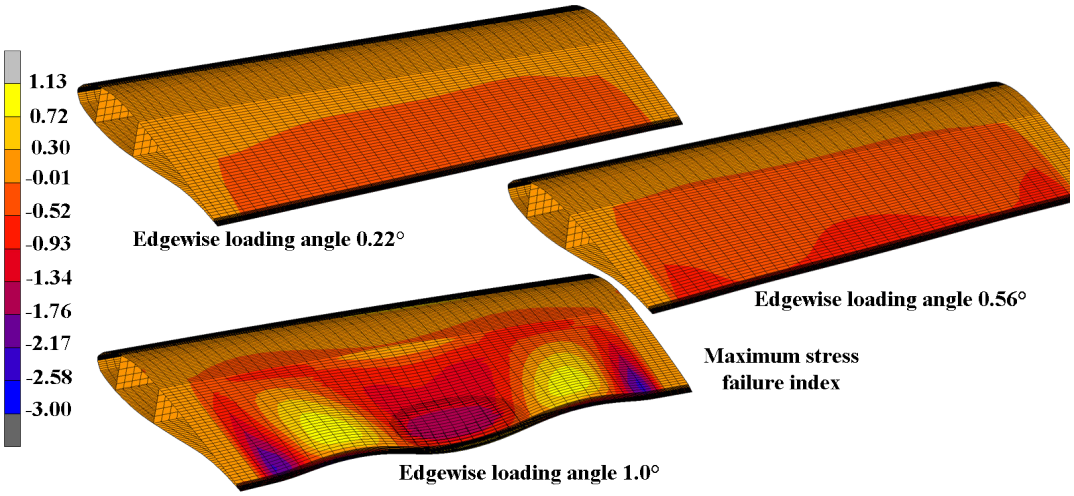

Figure 11: FE model maximum stress failure index at different load intervals.

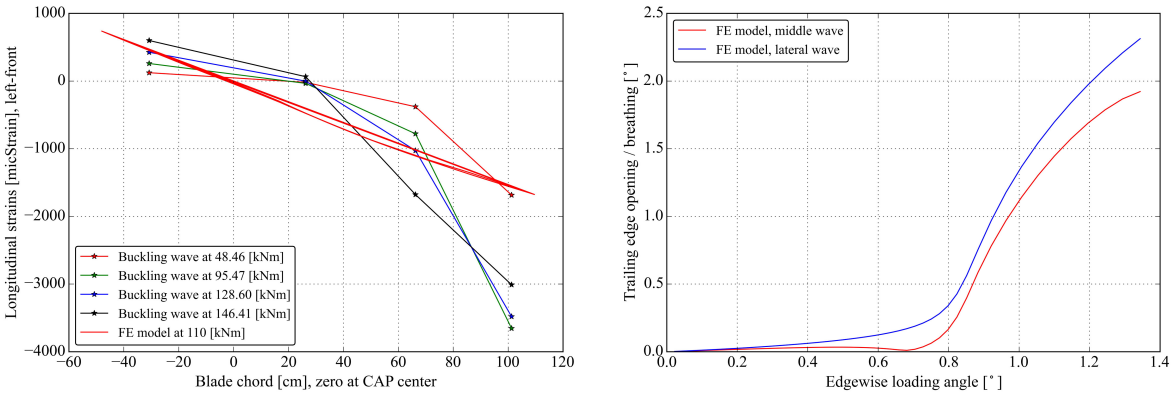

Figure 12: Transverse strain (in X axis) versus chord position (X axis), strain gauges 001F000, 002F000, 003F000, 013F000 (left plot) plus model strains at model buckling load. Trailing edge opening angle versus edgewise loading angle (right plot).

5 CONCLUSIONS

A sub-component test setup for wind turbine blades segments was proposed constructed and successfully applied. The test setup assesses the behaviour of wind turbine blade sections loaded with an edgewise moment. Static tests were carried out for a 3x2 meters blade section applying an edgewise moment until failure. During the test, the sub-component showed the formation of a buckling wave along the trailing edge until the fracture failure of the thick adhesive trailing edge joint. The static test

was evaluated using an FE model where edgewise stiffness and longitudinal strains showed a close agreement. Moreover, during the test, the buckling wave and reference strain profiles at different locations were measured. The adhesive joint failure was related to the edgewise moment and the formation of the buckling wave. The sub-component test setup allows testing full scale blade segments obtained directly from sectioning a blade. Therefore manufacturing defects and in-field conditions are included. Further work is on-going on the adhesive joint modelling and on the evaluation of the fatigue tests results using the same test setup configuration.

ACKNOWLEDGEMENTS

The authors acknowledge the contribution of the IRPWind and SLOWind projects to motivate and partly fund this research. The authors also acknowledge DTU and dr. Kim Branner for providing the blades sections and the feedbacks of IWES, CRES and CENER as IRPWind members.

REFERENCES

[1] M. Reder, E. Gonzalez, and J. J. Melero, "Wind Turbine Failure Analysis - Targeting current problems in Failure Data Analysis," *J. Phys. Conf. Ser.*, vol. 753, no. 72027, 2016.

[2] M. Wilkinson, B. Hendriks, F. Spinato, E. Gomez, H. Bulacio, P. Tavner, Y. Feng, and H. Long, "Methodology and Results of the Reliawind Reliability Field Study," *Eur. Wind Energy Conf. (EWEC 2010)*, no. Ewec, p. 7, 2010.

[3] S. Sheng and NREL, "Report on Wind Turbine Subsystem Reliability - A Survey of Various Databases," *NREL/PR-5000-59111,National Renew. Energy Lab.*, 2013.

[4] B. Attaf, *Recent Advances in Composite Materials for Wind Turbine Blades*. The World Academic Publishing Co. Ltd., 2013.

[5] S. Ataya and M. M. Z. Ahmed, "Damages of wind turbine blade trailing edge: Forms, location, and root causes," *Eng. Fail. Anal.*, 2013.

[6] M. A. Eder, R. D. Bitsche, and F. Belloni, "Effects of geometric non-linearity on energy release rates in a realistic wind turbine blade cross section," *Compos. Struct.*, vol. 132, pp. 1075–1084, 2015.

[7] M. A. Eder, R. D. Bitsche, M. Nielsen, and K. Branner, "A practical approach to fracture analysis at the trailing edge of wind turbine rotor blades," *Wind Energy*, vol. 17, no. 3, pp. 483–497, 2014.

[8] L. T. T. Data, M. Nielsen, F. M. Jensen, P. H. Nielsen, K. Martyniuk, A. Roczek, T. Sieradzan, V. Roudnitski, P. Kucio, R. Bitsche, P. Andresen, T. Lukassen, Z. Andrlová, K. Branner, C. Bak, M. Mcgugan, H. Knudsen, A. B. Rasmussen, J. J. Rasmussen, V. J. Wedel-heinen, A. M. Nielsen, H. Per, B. Kallesøe, T. Lindby, F. Sørensen, C. Jensen, U. Uldahl, and B. Rasmussen, "Full scale test of SSP 34m blade, edgewise loading LTT. Data report 1," 2010.

[9] P. U. Haselbach and K. Branner, "Initiation of trailing edge failure in full-scale wind turbine blade test," *Eng. Fract. Mech.*, vol. 162, pp. 136–154, 2016.

[10] K. Branner, P. Berring, and P. U. Haselbach, "Subcomponent testing of trailing edge panels in wind turbine blades," in *ECCM17 - 17th European Conference on Composite Materials*, 2016, no. June.

[11] F. Sayer, A. Antoniou, and A. Van Wingerde, "Investigation of structural bond lines in wind turbine blades by sub-component tests," *Int. J. Adhes. Adhes.*, vol. 37, pp. 129–135, 2012.

[12] M. Rosemeier, F. Lahuerta, K. Branner, and A. Antoniou, "Subcomponent testing of wind turbine blades," in *IRPWind conference (Amsterdam)*, 2016.

[13] P. U. Haselbach and K. Branner, "Effect of Trailing Edge Damage on Full-Scale Wind Turbine Blade Failure," in *20th International Conference on Composite Materials*, 2015, no. July, pp. 19–24.

[14] M. A. Eder and R. D. Bitsche, "Fracture analysis of adhesive joints in wind turbine blades," *Wind Energy*, vol. 18, no. 6, pp. 1007–1022, 2015.

[15] P. U. Haselbach, "Ultimate Strength of Wind Turbine Blades under Multiaxial Loading,"

Technical University of Denmark, 2015.
[16] F. Lahuerta, "Buckling tests on trailing edges. Preliminary FE. Hinge at the middle of the CAP. WMC-2016-007-cc," Knowledge Centre WMC, Wieringerwerf, 2016.
[17] G. D. de Winkel, *YouTube video: Wind turbine rotor blade trailing edge test to failure, https://www.youtube.com/watch?v=6pM6SlzNooQ&t=1s*. 2016.
[18] P. U. Haselbach and K. Branner, "Initiation of trailing edge failure in full-scale wind turbine blade test," *Eng. Fract. Mech.*, vol. 162, pp. 136–154, 2016.
[19] D. Samborsky, A. Sears, J. Mandell, and P. Agastra, "Mixed Mode Static and Fatigue Crack Growth in Wind Blade Paste Adhesives," *52nd AIAA/ASME/ASCE/AHS/ASC Struct. Struct. Dyn. Mater. Conf.*, no. mode I, pp. 1–19, 2011.